ADVANCED MATERIALS

Supporting Information

for *Adv. Mater.*, DOI: 10.1002/adma.201801984

Interlayer-Spacing-Regulated $VOPO_4$ Nanosheets with Fast Kinetics for High-Capacity and Durable Rechargeable Magnesium Batteries

Limin Zhou, Qi Liu, Zihe Zhang, Kai Zhang, Fangyu Xiong, Shuangshuang Tan, Qinyou An, Yong-Mook Kang, Zhen Zhou,* and Liqiang Mai**

Supporting Information

Interlayer Spacing Regulated $VOPO_4$ Nanosheets with Fast Kinetics for High-Capacity and Durable Rechargeable Magnesium Batteries

Limin Zhou, Qi Liu, Zihe Zhang, Kai Zhang, Fangyu Xiong, Shuangshuang Tan, Qinyou An, Yong-Mook Kang, Zhen Zhou,* and Liqiang Mai**

Experimental Section

Material Synthesis: *Preparation of OH-$VOPO_4$ bulk.* The OH-$VOPO_4$ was obtained by a facile hydrothermal method. First of all, 2.4 g V_2O_5 powders and 13.3 mL concentrated H_3PO_4 were added successively into 57.7 mL of deionized H_2O following by magnetic stirring for 2 h. Afterwards, the mixed solution was transferred into a 100 mL Teflon vessel and sealed in a stainless steel autoclave and then heated at 120 ˚C for 16 h. The bright-yellow product was collected via washing with deionized water and acetone and drying at 60 ˚C under vacuum.

Intercalation of PA molecules into $VOPO_4$ nanosheets (PA-$VOPO_4$). The intercalation composite was synthesized by ultrosonicated exfoliation and self-assembly procedure. In a typical exfoliation process, 100 mg OH-$VOPO_4$ bulk was dispersed in 7 mL isopropanol, and then the solution was sonicated for 30 min. After centrifugation, the exfoliation sheets were added into phenylamine solvent for 24 h of stirring. The dark-green PA intercalated $VOPO_4$ samples were further washed with acetone for three times, and dried in vacuum at 60 ˚C for

overnight. Besides, the tap density is valuated to be 0.7659 g cm^{-3} for PA-$VOPO_4$ through simple ultrasound treatment.

Preparation of all phenyl complex (APC) electrolyte. The all phenyl complex (APC) electrolyte was prepared in argon-filled glove box (< 1 ppm of water and oxygen) according to previous literature.[1] Specifically, 0.667 g aluminum chloride powder ($AlCl_3$, ultradry, 99.99 %) was slowly dissolved into 15 mL tetrahydrofuran (THF, anhydrous, 99.9 %, and dried by molecular sieves) for stirring 12 h. Then the above solution was slowly added into 5 ml phenyl magnesium chloride solution (2 M, PhMgCl/THF solution) for another 12 h of vigorous stirring to form APC electrolyte. The concentration of the as-prepared APC electrolyte is 0.25 M.

Material Characterization: The structure of the as-prepared samples was characterized by powder X-ray diffraction (XRD) patterns collected on a Bruker AXS D8 Advance powder X-ray diffractometer using Cu Kα radiation (λ = 1.5418). The geometric morphology of the samples was divulged by field-emission scanning electron microscope (FESEM, JEOL, JSM-7100F) and transmission electron microscope (TEM, JEOL 2100F). The elemental valence was analyzed by X-ray photoelectron spectroscopy on an ESCALAB 250 Xi spectrometer (XPS, VG Scientific Co., UK). The TG analysis was conducted on a NETZSCH-STA449c/3/G thermoanalyzer under an air atmosphere from 25 to 800 ˚C with a heating rate of 5 ˚C min^{-1}.

Electrochemical Tests: The electrochemical performance was tested with CR2032 coin cells, assembled by metallic magnesium as both reference and counter electrode, glass fiber as separator, APC as the electrolyte, and $VOPO_4$ nanosheets as working electrode. In order to avoid the side reaction, molybdenum foil was placed on electrode materials to ensure no-contact between electrolyte and battery case.[2] The working electrode was prepared by mixing active materials (PA-$VOPO_4$ nanosheets or OH-$VOPO_4$ bulk), acetylene black (AB), and poly(tetrafluoroethylene) (PTFE) at a weight ratio of 6:3:1. Then cut into a small disk with a mass loading of 1.3-1.8 mg cm^{-2}. The as-prepared electrodes were dried under vacuum at 110 ˚C for 10 h. The galvanostatic discharge/charge tests were carried out on Land CT2001A battery test system within the voltage range of 0.3 - 2.4 V (vs. Mg^{2+}/Mg). Electrochemical impedance spectroscopy (EIS) measurement was performed on Autolab electrochemical workstation with the frequency from 100 KHz to 100 mHz. According to the literature reported, 18.7 μL cm^{-2} of electrolyte is needed to match 1 mAh cm^{-2} of areal capacity when using $MgCl_2$ with 1.0 M concentration.[3] While commercial separators (300 μm thickness and 80 % porosity) may accommodate 24 μL cm^{-2} of electrolyte, which is enough for chloride ions to involve in $MgCl^+$ insertion process. Thus, it is possible to assemble the cells based on the practical ratio between electrolyte volume and electrode surface.

Computational details: First-principles computations based on density functional theory (DFT) were performed by using projected augmented wave (PAW)[4,5] pseudopotentials and

the Perdew–Burke–Ernzerholf (PBE)[6] exchange–correlation functional as implemented in Vienna ab initio simulation package (VASP) [5]. A 450 eV kinetic energy cutoff was used in all the computations. We performed the computations in a 2×2×1 $VOPO_4$ supercell. To simulate the interlayer spacing expanded by aniline intercalation, the lattice constant of *z*-axis was fixed to 14.24 Å as achieved by XRD. Therefore, a 3×3×2 Monkhorst-Pack k-point mesh was chosen for the sampling in the Brillouin zone.[7] The DFT-D3 method with Becke-Johnson damping was also adopted to better evaluate the van der Waals interactions.[8,9] In order to investigate the Mg^{2+} and $MgCl^{+}$ diffusion dynamics between $VOPO_4$ layers, we used the climbing-image nudged elastic band (CI-NEB)[10,11] method to calculate their migration pathways and the corresponding energy profiles.

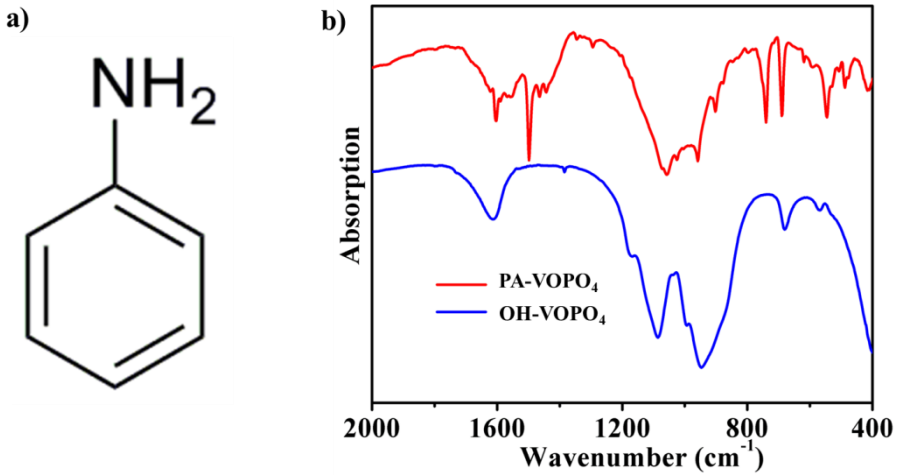

Figure S1. The molecule structure of phenyl-amine (PA) and (b) FTIR spectra of OH-$VOPO_4$ bulk and PA-$VOPO_4$ nanosheets**.**

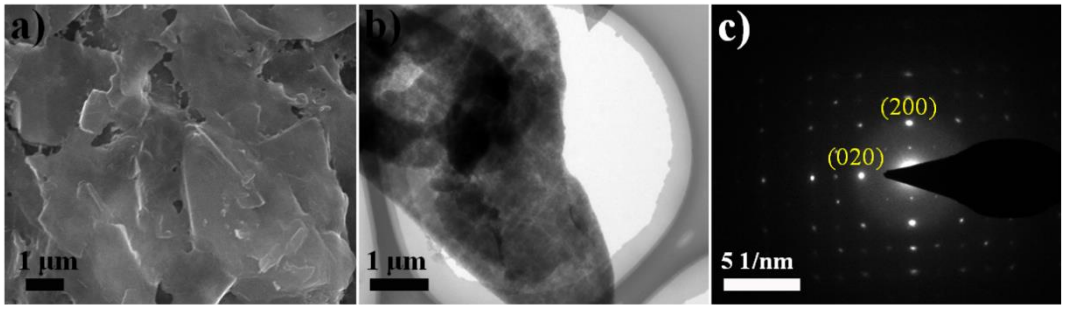

Figure S2. (a) SEM, (b) TEM, and (c) SAED of the OH-$VOPO_4$ bulk**.**

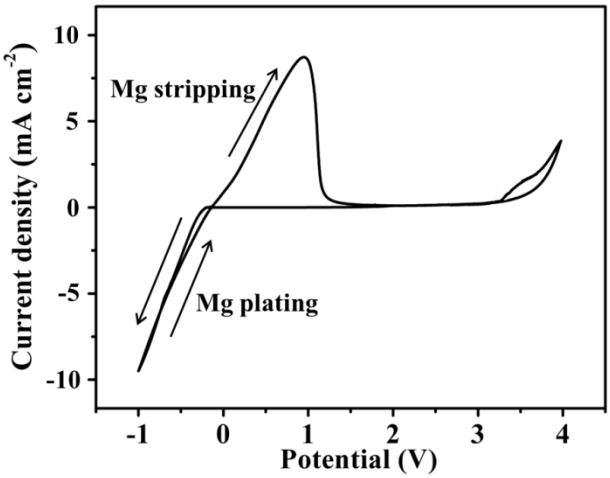

Figure S3. Cyclic voltammograms (CV) profile of APC electrolyte based on the counter and reference electrodes of magnesium foil and working electrode of platinum wire in three-electrode system at a scan rate of 25 mV s^{-1}.

We can see that the overpotential for Mg deposition is close to that of previous literature reported,[1] and the stripping/plating efficiency is ~100 %. Besides, the available electrochemical window of the solution is below 3.2 V due to the anodic limitation.

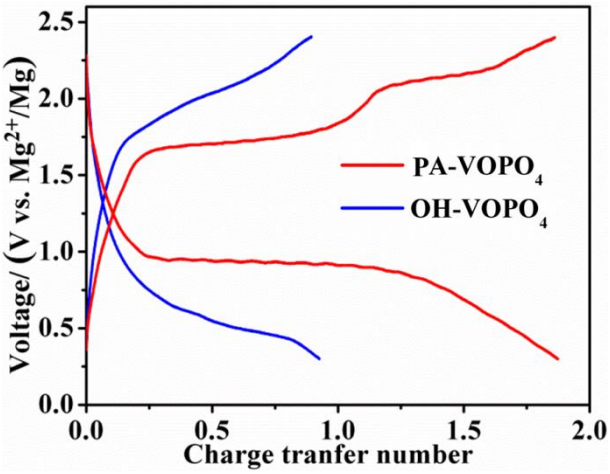

Figure S4. The plot of voltage vs. charge transfer number of the OH-$VOPO_4$ bulk and PA-$VOPO_4$ nanosheets at 100 mA g^{-1} and 50th cycle**.**

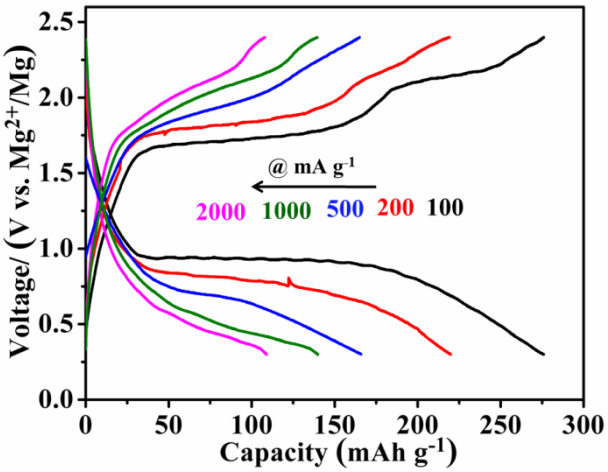

Figure S5. Charge/discharge curves of the PA-$VOPO_4$ nanosheets at different current densities.

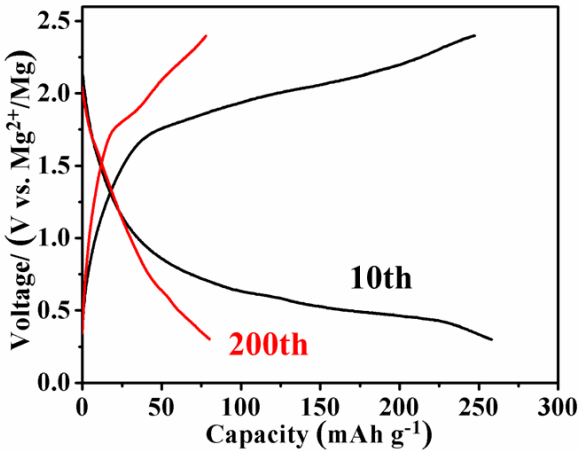

Figure S6. Charge/discharge curves of the OH-$VOPO_4$ bulk at 100 mA g^{-1}**.**

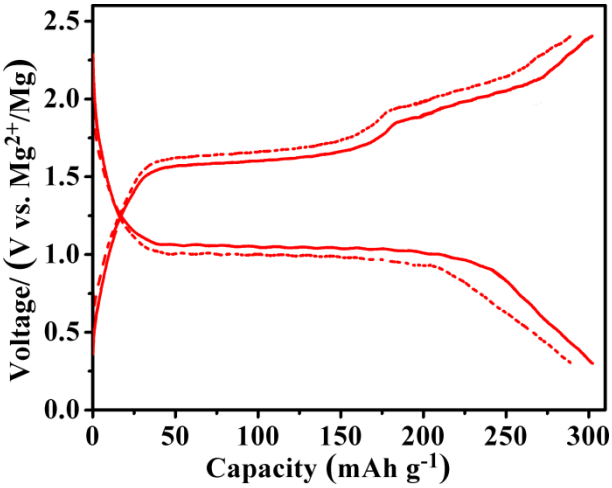

Figure S7. Charge/discharge curves of the PA-$VOPO_4$ nanosheets at 100 mA g^{-1} and 10th cycle measured at 35 and 50 ˚C**.**

We can see that the capacities of PA-$VOPO_4$ increase to 288 and 302 mAh g^{-1} at 35 and 50 ˚C, respectively. And the overpotenial of PA-$VOPO_4$ gradually decreases at elevated temperature, illustrating the ion diffusion has obviously positive correlation with the operated temperature.

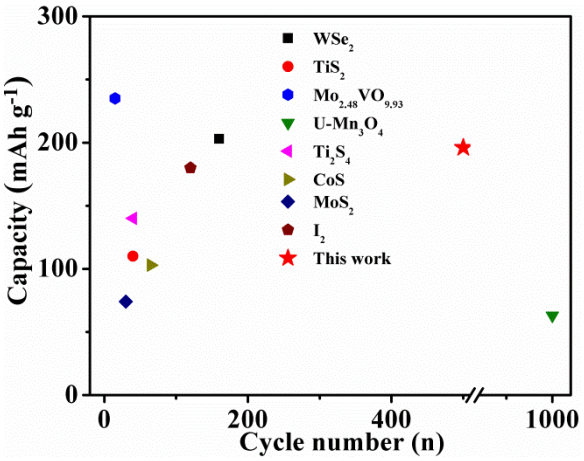

Figure S8. Comparison of cycling performance with other Mg-storage materials.

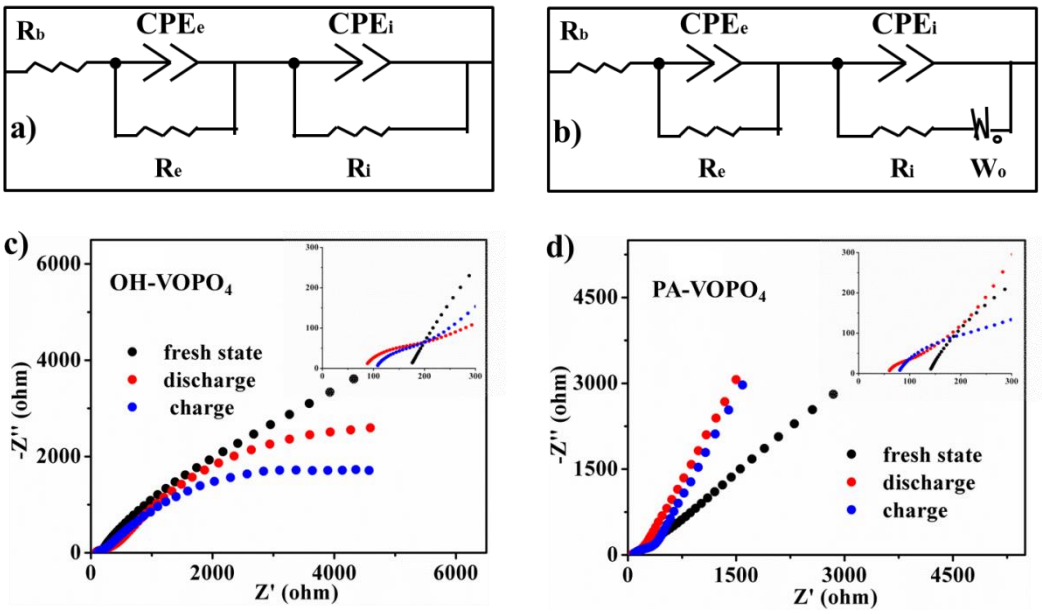

Figure S9. Equivalent circuits and the Nyquist plots of (a,c) OH-$VOPO_4$ and (b,d) PA-$VOPO_4$ electrodes at different cell states.

There is no straight line viewed for the OH-$VOPO_4$ bulk in the frequency range tested, reflecting sluggish electrode behavior. For the PA-$VOPO_4$ nanosheets, the obviously decreased R_e and R_i suggest that working cation of PA-$VOPO_4$ demonstrates low polarization and is not prone to trapped in the host, beneficial for good rate capability and long cycle life.

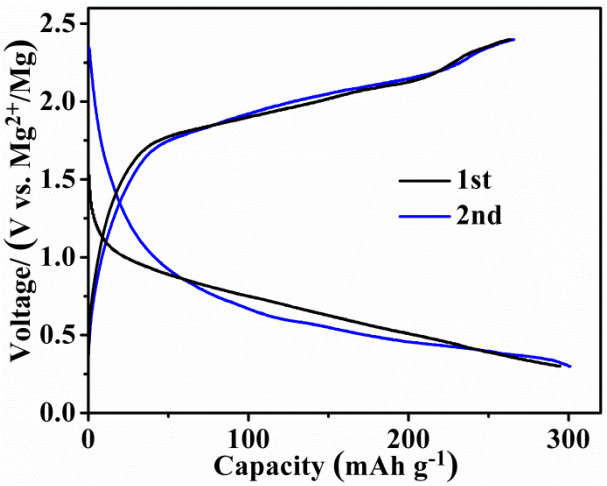

Figure S10. Charge/discharge curves of the OH-$VOPO_4$ bulk at 100 mA g^{-1} and 1st, 2nd cycles, illustrating the irreversible insertion/deinsertion reaction of OH-$VOPO_4$ electrode during initial charge/discharge process.

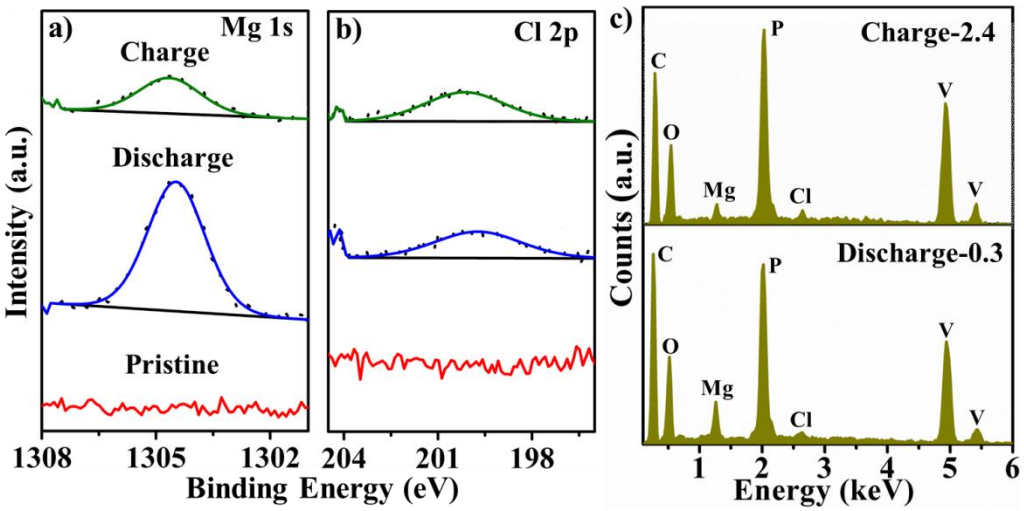

Figure S11. XPS spectra of (a) Mg 1s, (b) Cl 2p, and (c) EDS spectra for OH-$VOPO_4$ bulk at fully charged/discharged state.

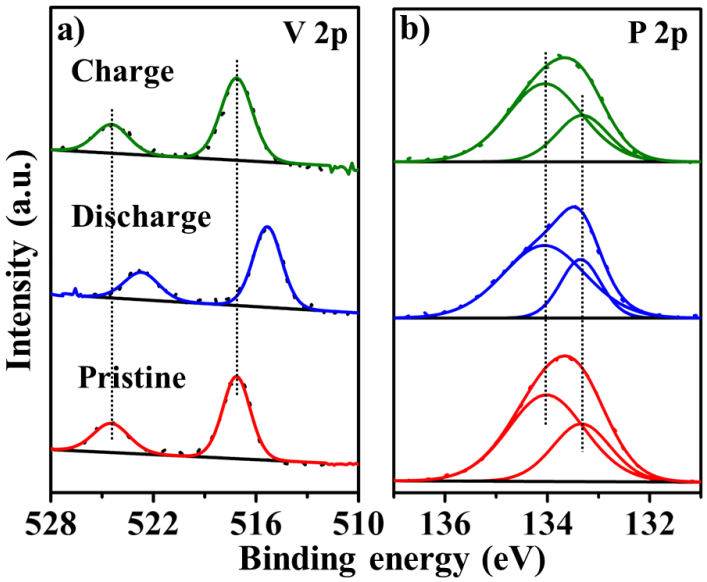

Figure S12. XPS spectra of (a) V 2p and (b) P 2p for the PA-$VOPO_4$ nanosheets and cycled electrode at fully charged/discharged state.

It can be seen that the peaks of V 2p located at 517.2, 524.5 eV slightly shift towards lower binding energy on discharging, illustrating the valence of V element decreases accompanied by cation insertion. Upon cation de-intercalation, the peak position of V element could recover back to initial state.

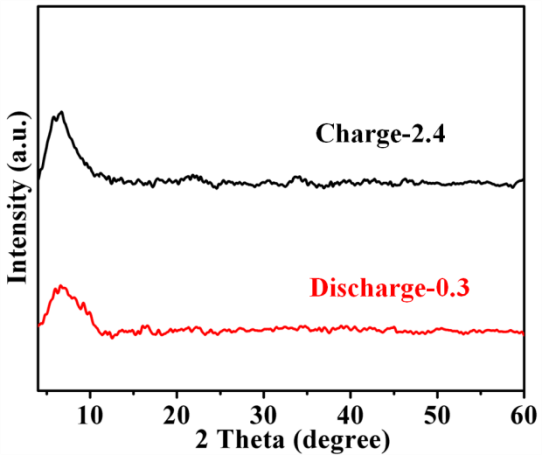

Figure S13. XRD patterns of the PA-$VOPO_4$ electrode at fully charged/discharged state after 50 cycles**.**

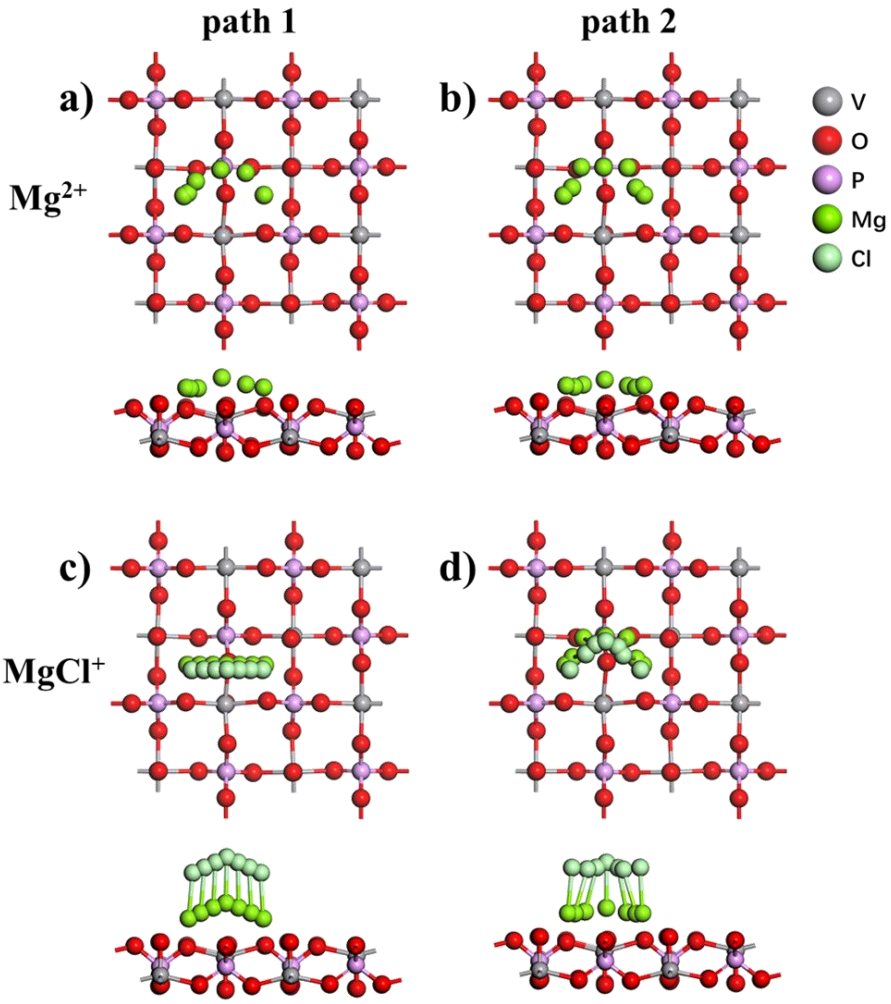

Figure S14. Top and side views of the migration paths of Mg^{2+} and $MgCl^+$ in PA-$VOPO_4$.

It is noticed that the path 2 for $MgCl^+$ shows abnormally high energy barrier, which might be attributed to the repulsion between the negatively charged O and Cl caused by the tilt configuration of $MgCl^+$ during the migration process.

Table S1. Summary of electrochemical performance of different host materials for rechargeable magnesium batteries.

Materials	**Voltage (V)**	**Capacity (mAh g^{-1})**	**Rate capability (mAh g^{-1})**	**Cycling capacity**	**Ref.**
PA-$VOPO_4$ nanosheets	0.95	310	310 (50 mA g^{-1}) 275 (100) 220 (200) 175 (500) 140 (1000) 109 (2000)	500 cycles, 192 mAh g^{-1}	**This work**
OH-$VOPO_4$ bulk	0.6	305	305 (50) 265 (100) 166 (200) 108 (500) 66 (1000) 43 (2000)	130 cycles, 121 mAh g^{-1}	This work
TiS_2	0.7	275	275 (12 mA g^{-1}) 250 (23.9) 140 (47.8)	40 cycles, 110 mAh g^{-1}	[12]
$Mo_{2.48}VO_{9.93}$	1.9	300	235(2) 114 (4)	15 cycles, 58.7 mAh g^{-1}	[13]
U-Mn_3O_4	0.8	100	103 (15.4) 84 (30.8) 76 (77) 67 (154) 58 (308) 37.5 (770) 22.5 (1540)	1000 cycles, 63 mAh g^{-1}	[14]
C-Ti_2S_4	1.2	200	200 (12) 195 (23.9) 190 (47.8)	40 cycles, 140 mAh g^{-1}	[15]
CoS	0.8	125	125 (50) 105 (100) 95 (150)	65 cycles, 103 mAh g^{-1}	[16]
Peo$_2$-MoS_2	0.65	82	70 (5) 62 (10) 55 (25) 44 (50) 38 (100)	30 cycles, 74 mAh g^{-1}	[17]

			30 (250) 22 (500)		
I_2	1.9	240	205 (52.75) 180 (105.5) 145 (158.25) 140 (211)	120 cycles, 180 mAh g^{-1}	[18]

Table S2. Selected voltage position for mass measurement of PA-$VOPO_4$ electrode.

Voltage (V)	0.36	0.45	0.5	0.59	0.68
Capacity (mAh g^{-1})	305	294	285	269	254
Electrode mass (mg)	3.03	2.99	2.97	2.91	2.86

Note: The mass of fresh PA-$VOPO_4$ electrode is ~2.20 mg.

Table S3. Selected voltage position for mass measurement of OH-$VOPO_4$ electrode.

Voltage (V)	0.36	0.45	0.5	0.59	0.68
Capacity (mAh g^{-1})	280	203	176	129	98
Electrode mass (mg)	2.60	2.53	2.49	2.46	2.46

Note: The mass of fresh OH-$VOPO_4$ electrode is ~2.46 mg.

Table S4. Characterization of PA-$VOPO_4$ nanosheets at different states based on EDS and ICP-OES analysis.

stage	**EDS**	**ICP-OES**
	Mg/Cl ratio	
Fully-discharged state	1.1	1.18
Fully-charged state	0.8	0.84

References

[1] O. Mizrahi, N. Amir, E. Pollak, O. Chusid, V. Marks, H. Gottlieb, L. Larush, E. Zinigrad, D. Aurbach, *J. Electrochem. Soc.* **2008**, *155*, A103.

[2] Y. Cheng, D. Choi, K. S. Han, K. T. Mueller, J. G. Zhang, V. L. Sprenkle, J. Liu, G. Li, *Chem. Commun.* **2016**, *52*, 5379.

[3] C. Liao, N, Sa, B. Key, A. K. Burrell, L. Cheng, L. A. Curtiss, J. T. Vaughey, J.-J. Woo, L. Hu, B. Pan, Z. Zhang, *J. Mater. Chem. A* **2015**, *3*, 6082.

[4] G. Kresse, D. Joubert, *Phys. Rev. B* **1999**, *59*, 1758.

[5] G. Kresse, J. Furthmüller, *Phys. Rev. B* **1996**, *54*, 11169.

[6] J. P. Perdew, K. Burke, M. Ernzerhof, *Phys. Rev. Lett.* **1996**, *77*, 3865.

[7] H. J. Monkhorst, J. D. Pack, *Phys. Rev. B* **1976**, *13*, 5188.

[8] S. Grimme, S. Ehrlich, L. Goerigk, *J. Comut. Chem.* **2011**, *32*, 1456.

[9] S. Grimme, J. Antony, S. Ehrlich, H. Krieg, *J. Chem. Phys.* **2010**, *132*, 154104.

[10] G. Henkelman, B. P. Uberuaga, H. Jónsson, *J. Chem. Phys.* **2000**, *113*, 9901.

[11] G. Henkelman, H. Jónsson, *J. Chem. Phys.* **2000**, *113*, 9978.

[12] X. Sun, P. Bonnick, L. F. Nazar, *ACS Energy Lett.* **2016**, *1*, 297.

[13] W. Kaveevivitchai, A. J. Jacobson, *Chem. Mater.* **2016**, *28*, 4593.

[14] L. Wang, K. Asheim, P. E. Vullum, A. M. Svensson, F. Vullum-Bruer, *Chem. Mater.* **2016**, *28*, 6459.

[15] X. Sun, P. Bonnick, V. Duffort, M. Liu, Z. Rong, K. A. Persson, G. Ceder, L. F. Nazar, *Energy Environ. Sci.* **2016**, *9*, 2273.

[16] D. He, D. Wu, J. Gao, X. Wu, X. Zeng, W. Ding, *J. Power Sources* **2015**, *294*, 643.

[17] Y. Liang, H. D. Yoo, Y. Li, J. Shuai, H. A. Calderon, F. C. Robles Hernandez, L. C. Grabow, Y. Yao, *Nano lett.* **2015**, *15*, 2194.

[18] H. Tian, T. Gao, X. Li, X. Wang, C. Luo, X. Fan, C. Yang, L. Suo, Z. Ma, W. Han, C. Wang, *Nat. Commun.* **2017**, *8*, 14083.